Gümüşhane University Journal of Science

Active contour-based tooth segmentation in radiographs using fuzzy logic and CNN

Bulanık mantık ve CNN kullanarak radyograflarda aktif kontur tabanlı diş bölütleme

Fatih DURMUS[1] iD **, Ferdi OZBILGIN[2]** iD **, Serap KARAGOL*[1]** iD

[1]*Ondokuz Mayıs University, Engineering Faculty, Department of Electrical and Electronics Engineering, 55100, Samsun*
[2]*Giresun University, Engineering Faculty, Department of Electrical and Electronics Engineering, 28200, Giresun*

Abstract

Radiographic imaging is a crucial tool frequently employed by dentists for initial diagnosis and treatment planning. However, these images often suffer from distortion or inaccuracies due to incorrect exposure settings, making it challenging to identify critical regions such as tooth roots and margins. This study addresses these issues by presenting two innovative methods for tooth segmentation from radiographs, aimed at isolating the tooth regions for better analysis. The first method utilizes fuzzy logic rules to detect edges within the radiographic images. These detected edges are then used as a mask for the Active Contour Method (ACM) to segment the teeth accurately. The second method involves the creation of a Convolutional Neural Network (CNN) for tooth segmentation. The segmentation performance of the CNN is further refined using the ACM, leveraging the initial segmentation as a mask. Both methods demonstrated notable results with varying performance metrics. Specifically, the Fuzzy-Based Active Contour Method achieved precision, recall, and F1 score values of 0.6246, 0.4169, and 0.50, respectively. In contrast, the CNN-Based Active Contour Method calculated accuracy and specificity values of 0.9706 and 0.9872, respectively. These findings indicate that both approaches have distinct strengths in different performance aspects. Our study suggests that these advanced segmentation techniques can significantly enhance the diagnostic capabilities of dental professionals by providing clearer images of tooth structures, aiding in the detection of issues such as root problems, fractures, and wear patterns. Implementing these methods either independently or in combination could lead to more accurate diagnoses and better patient outcomes. Future work could explore the integration of these techniques to leverage their complementary strengths, potentially leading to even greater segmentation accuracy and reliability.

Keywords: Active contour method, Convolutional neural network (CNN), Fuzzy logic rules, Teeth segmentation

Öz

Radyografik görüntüleme, diş hekimlerinin ilk teşhis ve tedavi planlamasında sıklıkla kullandığı önemli bir araçtır. Ancak, bu görüntüler bazen yanlış pozlama ayarlarından dolayı bozulabilir veya hatalı olabilir, bu da diş kökleri ve kenar bölgeleri gibi kritik bölgelerin tanımlanmasını zorlaştırır. Bu çalışma, radyografilerden diş segmentasyonu yaparak diş bölgelerinin izole edilmesini amaçlayan iki yenilikçi yöntem sunmaktadır. İlk yöntemde, radyografik görüntülerdeki kenarları tespit etmek için bulanık mantık kuralları uygulanmıştır. Tespit edilen bu kenarlar, Aktif Kontur Yöntemi (ACM) ile dişlerin doğru bir şekilde segmentasyonu için maske olarak kullanılmıştır. İkinci yöntemde ise, diş segmentasyonu için bir Konvolüsyonel Sinir Ağı (CNN) oluşturulmuştur. CNN'in segmentasyon performansı, başlangıçtaki segmentasyonun maske olarak kullanılmasıyla ACM ile daha da iyileştirilmiştir. Her iki yöntem de farklı performans metrikleri ile dikkate değer sonuçlar göstermiştir. Özellikle, Bulanık Tabanlı Aktif Kontur Yöntemi için doğruluk, geri çağırma ve F1 skoru değerleri sırasıyla 0.6246, 0.4169 ve 0.50 olarak elde edilmiştir. Buna karşılık, CNN Tabanlı Aktif Kontur Yöntemi için doğruluk ve özgüllük değerleri sırasıyla 0.9706 ve 0.9872 olarak rapor edilmiştir. Bu bulgular, her iki yaklaşımın da farklı performans kriterlerinde belirgin güçlü yönlere sahip olduğunu göstermektedir. Çalışmamız, bu ileri düzey segmentasyon tekniklerinin, diş yapılarının daha net görüntülerini sağlayarak diş hekimlerinin teşhis yeteneklerini önemli ölçüde artırabileceğini önermektedir. Bu yöntemlerin bağımsız olarak veya birlikte uygulanması, daha doğru teşhislere ve daha iyi hasta sonuçlarına yol açabilir. Gelecekteki çalışmalar, bu tekniklerin entegrasyonunu araştırarak, tamamlayıcı güçlü yönlerini kullanarak daha yüksek segmentasyon doğruluğu ve güvenilirliğine ulaşmayı hedefleyebilir.

Anahtar kelimeler: *Aktif kontur yöntemi, Evrişimli sinir ağı (CNN), Bulanık mantık kuralları, Diş segmentasyonu*

*Serap KARAGOL; serap.karagol@omu.edu.tr

1. Introduction

Radiography is an imaging technique that uses X-rays, gamma rays, or ionizing and non-ionizing radiation to show the internal structure of objects (Adejoh et al., 2016). In dental practice, radiographs serve as diagnostic tools for assessing the oral cavity's health, encompassing the condition of teeth, gums, jaw, and bone structure (Kumar et al., 2021). This allows dentists to treat invisible problems such as early tooth decay, gum disease, and abscesses. Additionally, dental radiographs find utility in personal identification, where biometric systems play a crucial role (Mitra, 2021). Common biometric features include fingerprints, facial features, voice patterns, and iris scans. While these features can be effectively utilized, they are susceptible to errors and may fail under adverse conditions or significant incidents. Consequently, such biometric characteristics often prove inadequate in detecting remains afflicted by severe harm resulting from accidents like fires or earthquakes. Notably, dental images played a pivotal role in expeditiously identifying numerous individuals during the 2004 tsunami in Thailand (Bozkurt & Karagol, 2020). Information derived from dental features emerges as more reliable for identification purposes compared to other biometric properties due to their durability.

Image segmentation is the process of dividing a digital image into multiple segments. Segmentation of teeth involves separating the tooth region from other areas, but this process is complex due to changes in shape and density (Polizzi et al., 2023). Although image segmentation methods are generally used to locate objects and boundaries in images, they can be broadly divided into two categories: edge-based and pixel-based. In contrast with pixel-based segmentations, which classify pixels in a set of regions of an object, edge-based segmentations search for realistic contours of the object. The published literature contains numerous studies on the improvement of segmentation. Sezgin and Sankur categorized the segmentation methods according to characteristic features such as shape, histogram, threshold, and region-based (Sezgin et al., 2004). Gil Silva et al. also divided this classification into five groups: region-based, cluster-based, boundary-based, watershed-based and threshold-based (Silva et al., 2018). The classification of the groups is based on the methods listed in Table 1.

Table 1. Segmentation categories and segmentation methods

Category	Segmentation methods
Region based	Region growing, Region splitting and merging (Khalid, 2022)
Watershed	Marker-controlled watershed (Kaseva et al., 2022)
Boundary based	Sobel, Canny, Active Contour, Level-set (Hoang & Tran, 2021)
Thresholding based	Niblack, Basic global thresholding (Bruellmann et al., 2016)
Clustering based	Fuzzy C-means clustering (Hashemi et al., 2023)

The fuzzy logic theory has been successfully applied in many fields, such as threshold selection (Cheng et al., 2000), pattern recognition, computer vision (Thakkar et al., 2023), image enhancement (Cheng & Xu, 2002), image classification, image segmentation (Gomez et al., 2006). A wide variety of fields, including computer vision and image processing, rely on edge detection. There is a difference in gray color between edge pixels and adjacent pixels. However, the definition of "large" is quite fuzzy and depends on the particular applications. The edge of the image should be defined using fuzzy logic theory to remove this ambiguity and to minimize the blurring of the edge pixels of the image. For this purpose, a three-layer neural fuzzy network system is developed. It includes adaptive blur, edge detection and modified Hopfield neural network. Adaptive blur is a feedforward neural fuzzy network. It is used for blurring input models for edge detection and enhancement. A fuzzy If-Then inference rule approach that uses fuzzy templates (operators) to identify specific models of neighboring pixels is discussed in (Hu et al., 2007). Each pixel is defined as a variable, a bright or dark pixel, depending on its corresponding membership. Variables are then added using a fuzzy adder operator based on predefined templates. Finally, fuzziness is applied and all pixels of the image are classified as edge pixels or non-edge pixels. Different fuzzy templates for the detection operations can result in different fuzzy edge detectors suitable for different applications. Sixteen different sets of templates adapted from (Hu et al., 2007) were used in this study to detect white lines. In this paper, considering the continuity of edges, the fuzzy extraction rule If-Then is used, which can overcome the shortcomings of the above edge detection algorithms. This edge detection method was applied to the panoramic radiograph and an attempt was made to determine the edges of the teeth. CNN have been used for various applications, such as semantic segmentation (Long et al, 2015), image classification (Zhang et al., 2022), computer vision and in medical image segmentation and classification (Ramachandran et al., 2022). Active contours for image segmentation can be used both

boundary-based and region-based methods (Li et al., 2008). Some studies use only the active contour method (Jain & Chauhan, 2019), only fuzzy logic (Dhanachandra & Chanu, 2020), and only convolutional neural networks (Minnema et al., 2019).

In contrast to the existing literature, where hybrid methods combining different techniques are relatively scarce, this study explores the integration of fuzzy logic and convolutional neural networks (CNN) for active contour segmentation. The utilization of both fuzzy logic and CNN methods aims to enhance performance by leveraging the strengths of each approach. Specifically, fuzzy logic, with its capability to handle uncertainty and vagueness in image data, and CNNs, known for their powerful feature extraction and classification abilities, were combined to generate mask images for the active contour method. This hybrid approach is expected to offer improved accuracy and robustness in edge detection and image segmentation tasks, addressing the limitations observed in the use of singular methods. The combination of these techniques not only highlights the potential for performance enhancement but also paves the way for future research in hybrid methodologies within the field of image processing.

The rest of the paper is organized as follows. Section 2 presents the background information and the related algorithms on which this work is based. In Section 3, the performance of proposed method is evaluated and compared with a set of algorithms from the literature. Finally, Section 4 concludes this paper.

2. Material and method

Dental radiographs can be divided into panoramic, bitewing and periapical images, as shown in Figure 1 (Silva et al.,2018). Panoramic radiographs are used to view the entire mouth, which includes the mandible and maxilla. Periapical images provide information about the entire tooth area, including the tissue around the root apex, while bitewing images provide information about the roots. Many dental diseases can be detected with these images, including dental and bone abnormalities, tumors, cysts and infections.

Figure 1. Types of X-ray images: (a) panoramic X-ray, (b) bitewing X-ray, (c) periapical X-ray

2.1. Characteristics of the dataset

The dataset used in this study is obtained from Gil Silva et al. (Silva et al.,2018). This dataset contains 1,500 annotated panoramic X-ray images and represents the largest freely available resource for dental radiography research. Table 2 presents an overview of the dataset statistics, including image categories, treatment scenarios, the total number of images per category, and the average number of teeth per category. The image categories range in size from 45 to 457 images.

Table 2. Categorization of dataset images and average number of teeth per category

Number	Category	Treatment	Total number of images	Average teeth
1	All teeth	Restoration and dental appliance	73	32
2	All teeth	Only restoration	220	32
3	All teeth	Only dental appliance	45	32
4	All teeth	No restoration or dental appliance	140	32
5	Negligible	Dental implant	120	18
6	More than 32 teeth	Negligible	170	37
7	Missing teeth	Restoration and dental appliance	115	27
8	Missing teeth	Only restoration	457	29
9	Missing teeth	Only dental appliance	45	28
10	Missing teeth	No restoration or dental appliance	115	28

2.2. Determining ROI

In order to evaluate the segmentation methods, only regions of interest (ROIs) were considered. The image in Figure 2(b) is a segmented binary image of the oral region from the dataset. Manually created mask images are included in the dataset. The image in Figure 2(c) was obtained by multiplying the original image in Figure 2(a) by the image in Figure 2(b) pixel by pixel. These steps were performed for all images used in the study.
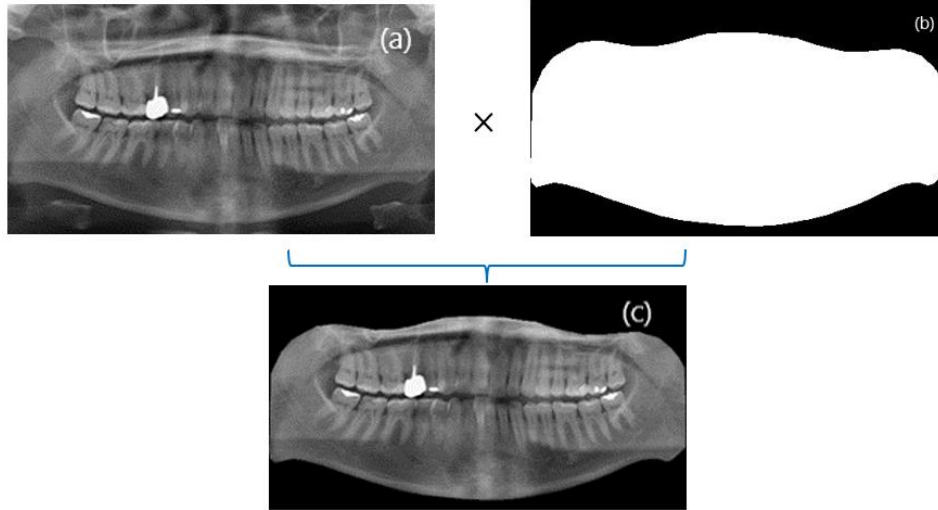
Figure 2. Images in dataset a) panoramic X-ray image b) binary image obtained by buccal annotation c) ROI image

2.3. Active contour model

An active contour model, commonly known as a 'snake,' is used for segmenting an object's boundaries from other regions within an image. Since its introduction by Kass, Witkin, and Terzopoulos in 1988, this model has seen extensive applications (Kass et al., 1988). It is a model-based method and a special case of the deformable models. In deformable models, segmentation is performed under the action of internal, external and image forces.

In the original active contour model algorithm, the snake is a parametric contour geometrically located in the image plane $(x,y) \in \Re^2$ and represented by x and y coordinate values. The representation of a two-dimensional contour is formulated with a parametric domain element s $\in$ [0, 1] as expressed in (Thias et al., 2019):

$$v(s) = (x(s), y(s))^T \tag{1}$$

The energy of the contour is calculated as follow:

$$E(v) = S(v) + P(v) \tag{2}$$

The provided function consists of two terms: the first term corresponds to the internal deformation energy, while the second term is associated with the image properties. $S(v)$ is characterized by the tension and flexibility distortions of the contour and provided in Eq. (3). The terms $w_1(s)$ and $w_2(s)$ controls the contour tension and contour stiffness respectively (Thias et al., 2019).

$$S(v) = \int_0^1 w_1(s) \left| \frac{\partial v}{\partial s} \right|^2 + w_2 \left| \frac{\partial^2 v}{\partial s^2} \right|^2 ds \tag{3}$$

The term $P(v)$ in Eq. (4) refers to the image and is controlled by the image. This term guides the algorithm to focus on image details, such as lines and edges

$$P(v) = \int_0^1 P(v(s)) ds \tag{4}$$

2.4. Fuzzy logic rules

Machine vision, computer vision, and image processing are interdisciplinary fields uzing edge detection to segment images and extract data. In this study, an edge detection method based on fuzzy rules and edge continuity is employed. Additionally, the fuzzy logic-based edge detection method is compared with conventional edge detection methods such as Canny, Sobel, and Prewitt. In contrast to other edge detectors, the proposed edge detection method is very insensitive to noise and can provide good results even in severe edge noise environments. The rules outlined in (Hu et al., 2007) were applied in performing edge detection with fuzzy logic. The main principle followed here is edge continuity. The pixels are sampled in the form of 3×3 windows, as shown in Figure 3. According to the rule, an edge is defined as the difference in image values between sampled edge pixels and surrounding pixels. If there is a situation that deviates from the rule, it is interpreted that the marked pixel is not an edge pixel.

3	4	5
2	Q	6
1	8	7

Figure 3. 3x3 window

The gray level difference of a pixel with its neighbor pixel x_k is defined as:

$$x_k = Gray_{Diff(Q,k)} = \text{Gray}(k) - \text{Gray}(Q), \quad k = 1,2,\dots,8 \tag{5}$$

where $\text{Gray}(Q)$ is the grey level of the central pixel Q, and $\text{Gray}(k)$ is the grey level of the neighbor pixel k. The membership functions shown in Figure 4 associated with the gray level difference x are defined as Dark(x) (D(x)) and Bright(x) (B(x)) (Hu et al., 2007). Here, the c value is half of the standard deviation in the image. For any grey level difference x, the membership functions Bright and Dark are defined in Eq. (6) and Eq . (7).
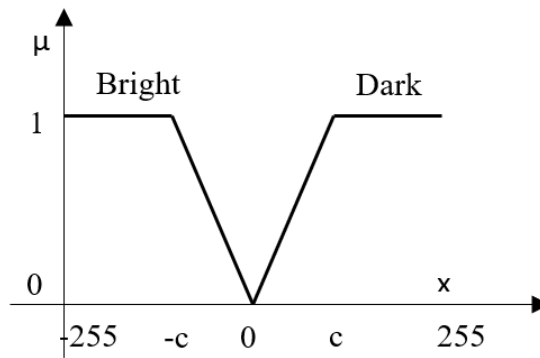
Figure 4. Graph of membership function

$$\text{Bright}(x) = \begin{cases} 0, & x \leq 0 \\ \frac{x}{c}, & 0 < x < c \\ 1, & x \geq c \end{cases} \tag{6}$$

$$\text{Dark}(x) = \begin{cases} 0, & x \leq 0 \\ -\frac{x}{c}, & -c < x < 0 \\ 1, & x \leq -c \end{cases} \tag{7}$$

If the center (Q) pixel and the pixels marked with the "?" sign are accepted as edges. There are eight different directions of the edge. Fuzzy Rule templates generated by these edge states are shown in Figure 5.

Figure 5. Fuzzy If-Then inference rules R1-R8

As examples of If-Then rules in fuzzy logic R1 is written as in Eq. (8). The R2-R8 rules can be expressed similarly (Hu et al., 2007).

$$R_1(Q) = D\left(\text{Gray}_{\text{Dif}(Q,1)}\right) \cap D\left(\text{Gray}_{\text{Dif}(Q,2)}\right) \cap D\left(\text{Gray}_{\text{Dif}(Q,8)}\right) \cap B\left(\text{Gray}_{\text{Dif}(Q,4)}\right) \cap B\left(\text{Gray}_{Dif(Q,5)}\right) \cap$$
$$B\left(\text{Gray}_{\text{Dif}(Q,6)}\right) \tag{8}$$

In Eq. (8), 'B' represents the membership function of 'Bright,' as defined in Eq. (6), and 'D' represents the membership function of 'Dark,' as defined in Eq. (7). According to Rule 1, if the neighboring pixels (4, 5, 6) are bright, and pixels (1, 2, 8) are dark, then the central pixel Q is designated as an edge pixel, as illustrated in Eq. (8). It is possible to discuss Rules 2–8 in a similar manner.

For edge detection, these eight rules were not sufficient for noisy images and gray scale images. Consequently, an additional set of eight rules was introduced based on the continuity principle to determine whether the pixels marked with "?" qualify as edge pixels. Figure 6 illustrates Rule 9 as an example of these rules, and this rule template was created to apply to pixel number 3 and pixel number 7 in Region 1. Similarly, Rules 10–16 can be derived.
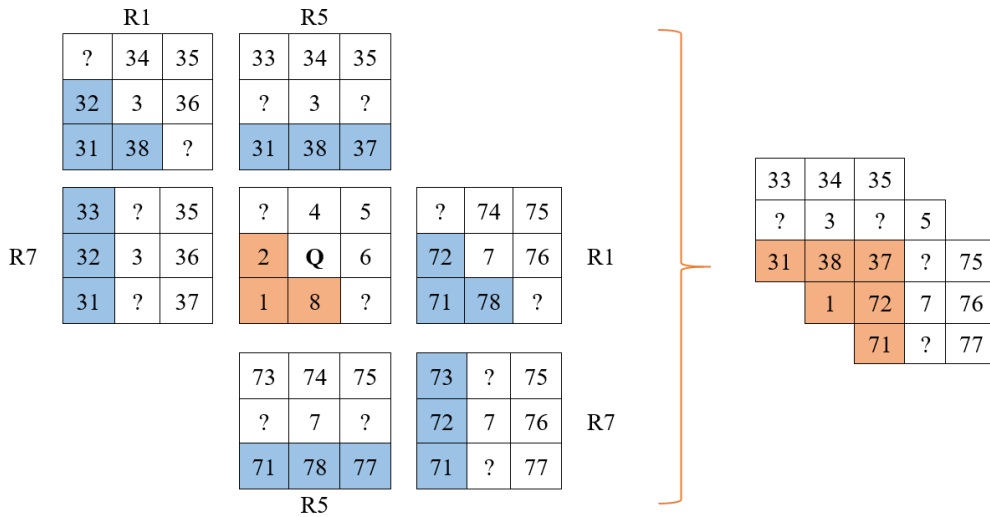
Figure 6. The template of Rule 9

As examples of If-Then rules in fuzzy logic R₉ is written as follow (Hu et al., 2007):

$$R_9(Q) = R_1(Q) \cap \left(\left(R_1(3) \cup R_5(3) \cup R_7(3)\right) \cap_1 \overline{\left(R_2(3) \cup R_3(3) \cup R_4(3) \cup R_6(3) \cup R_8(3)\right)}\right) \cap$$
$$\left(\left(R_1(7) \cup R_5(7) \cup R_7(7)\right) \cap_1 \overline{\left(R_2(7) \cup R_3(7) \cup R_4(7) \cup R_6(7) \cup R_8(7)\right)}\right) \tag{9}$$
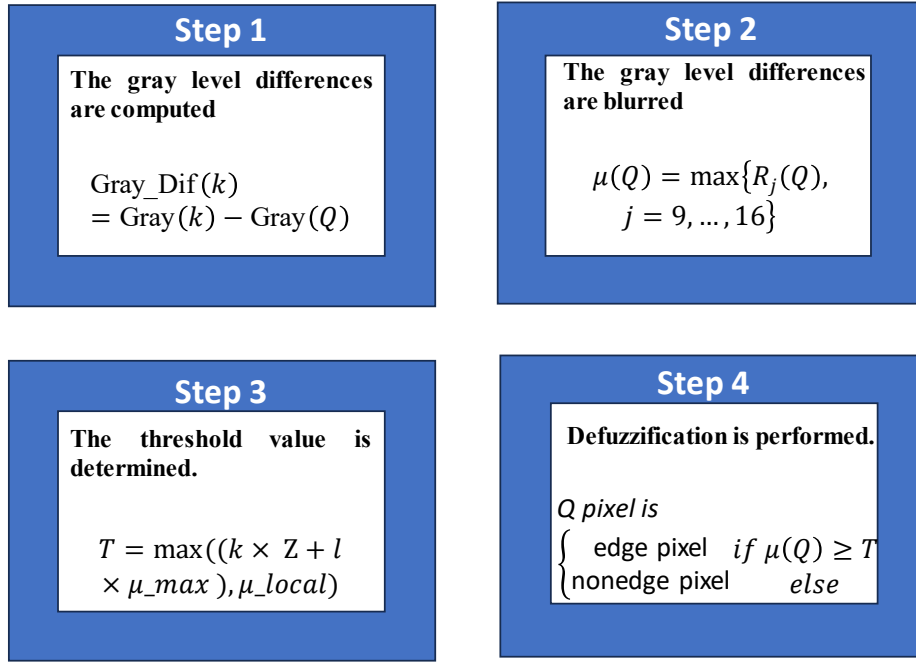
Here "∪" is the MAX operator and "∩" is a weighted arithmetic mean operator. The utilization of MIN as a collector operator is avoided in this context due to its robustness and sensitivity to noise. The weight assigned

to a pixel is determined as follows: if the pixel is in the vertical or horizontal direction, its weight is 2; if it's in the transverse direction, its weight is 1. Vertical and horizontal pixels have a greater impact on the central pixel than transversal neighbors. "∩₁" is the strongest MIN collector, i.e., only the minimum value is usually considered. It emphasizes a strong boundary continuity condition and can avoid noise. "‾" is an ordinary complement operator. After applying the fuzzy If-Then extraction rules, the fuzzy edge image should be defuzzified. A common method of defuzzing is centroid defuzzification :

$$Z = \frac{\int \mu(z)z\,dz}{\int \mu(z)\,dz} \tag{10}$$

where μ (z) is the membership function.

Figure 7 shows the defuzification steps of Q pixel.

Step 1

The gray level differences are computed

$$\text{Gray\_Dif}(k) = \text{Gray}(k) - \text{Gray}(Q)$$

Step 2

The gray level differences are blurred

$$\mu(Q) = \max\{R_j(Q), \quad j = 9, \dots, 16\}$$

Step 3

The threshold value is determined.

$$T = \max((k \times Z + l \times \mu\_max), \mu\_local)$$

Step 4

Defuzzification is performed.

Q pixel is
$$\begin{cases} \text{edge pixel} & if\ \mu(Q) \geq T \\ \text{nonedge pixel} & else \end{cases}$$

Figure 7. Illustration of defuzification steps of Q pixel

For each Q pixel, the algorithm is summarized as follows:

1. The gray level differences from the neighboring pixels are computed as in Eq. (11)

$$\text{Gray\_Dif}(k) = \text{Gray}(k) - \text{Gray}(Q), \quad k = 1,2, \dots, 8 \tag{11}$$

2. In the second step, the gray level differences corresponding to the "Bright(x)" and "Dark(x)" membership functions are blurred. The membership values are then computed according to the If-Then interference rules R_j (Q), $j = 9,\dots,16$ and the largest $R_j(Q)$ the value that satisfies the rule is selected according to Eq. (12):

$$\mu(Q) = \max\{R_j(Q), \quad j = 9, \dots, 16\} \tag{12}$$

3. In this step, the threshold value that defuzzifies the rules and values is determined.

$$T = \max\left((k \times Z + l \times \mu_{max}), \mu_{local}\right) \tag{13}$$

where μ_{max} is the maximum total membership value, Z is given in Eq. (10), and μ_{local} is the average membership value in 3×3 windows. k and l values were determined by trial and error in this study. A coefficient is accepted as correct if it has the highest accuracy.

4. In the final stage, defuzzification is performed as

$$Q\ pixel\ is \begin{cases} \text{edge pixel} & if\ \mu(Q) \geq T \\ \text{nonedge pixel} & else \end{cases} \tag{14}$$

2.4. Convolutional neural network

A Convolutional Neural Network (CNN) is a type of feedforward neural network that has been increasingly employed in recent years for classification, segmentation, and object detection in pattern recognition and computer vision (Cellegin et al., 2023). Operating on the principle of hierarchical learning, this method has demonstrated significant success. As the input data passes through multiple layers, there is a progressive decomposition of the desired information. The information is learned in finer detail as the network's layers deepen (Milletari et al., 2016). Figure 8 provides an illustration of a Convolutional Neural Network and its application in segmentation.
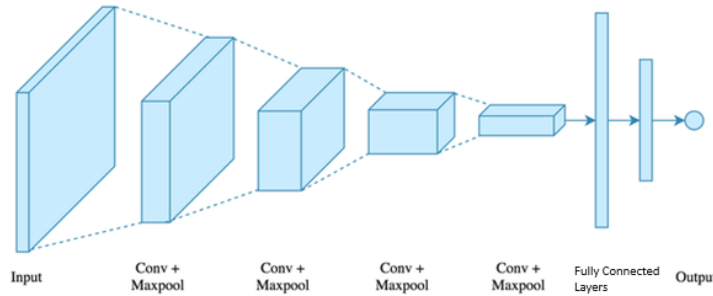
Figure 8. An example CNN architecture

CNNs typically contain a number of different components. These components are adapted according to the problem. The components are as follows;

Convolutional layer: In CNN, the convolutional layer is the main layer and contains a number of adaptive filters. These filters operate by conducting convolution operations instead of matrix multiplications in at least one layer.

Pooling: The pooling process involves the reduction of output size through functions such as averaging or selecting maximum values to combine the sub-ranges. Pooling involves subtracting a value by averaging or computing the maximum within a defined range. The application of pooling utilizes the sliding window method on the input, where the sliding window generates a value from the input field based on the specified pooling method, contributing to the output layer.

ReLu layer: Activation functions are an important factor for convolutional neural networks, and the rectified linear unit (ReLU) activation function is commonly utilized in deep neural network models. This layer possesses the significant property of setting negative input values to zero, as given in Eq. (15). This characteristic accelerates the learning process of the network when employing the ReLU function.

$$f(x) = \begin{cases} 0, & if\ x < 0 \\ x, & if\ x \geq 0 \end{cases} \tag{15}$$

Fully connected layer: The values generated by convolution and pooling are taken as input by this layer and processed as a number of classes in the output layer. Figure 9 shows the network architecture used in the study.
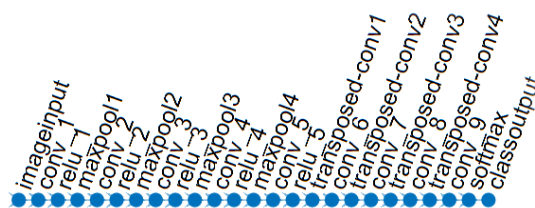
Figure 9. The CNN architecture used in the study

The proposed network architecture consists of 25 layers. A total of 154 data points, equivalent to 70% of the 220 data points in the dataset, were utilized as training data for the network. Performance analysis was performed by comparing the segmented image with the actual data. Additionally, an active contouring method based on the convolutional neural network was implemented, utilizing the active contouring results as a mask image. The segmentation performance was assessed through a comparative analysis between the images generated by this method and the actual data.

2.6. Performance evaluation

Metrics, such as accuracy (Eq. 16), specificity (Eq. 17), precision (Eq. 18), recall (Eq. 19) and F1 score (Eq. 20), were used to assess the performance of each segmentation method analyzed here:

$$\text{Accuracy} = \frac{TP+TN}{TP+FN+FP+TN} \tag{16}$$

$$\text{Specificity} = \frac{TN}{FP+TN} \tag{17}$$

$$\text{Precision} = \frac{TP}{TP+FP} \tag{18}$$

$$\text{Recall} = \frac{TP}{TP+FN} \tag{19}$$

$$\text{F1}_{\text{score}} = 2 \times \frac{\text{Precision} \times \text{Recall}}{\text{Precision}+\text{Recall}} \tag{20}$$

where TP refers to true positive results, FN refers to false negative results, FP refers to false positive results, and TP refers to true negative results. *Accuracy* is the ratio between correctly predicted observations and the total observation rate. A high value indicates high accuracy. *Specificity* is the ratio between the number of correctly predicted negative estimates and the total number of negatives. *Precision* is the ratio between the number of positive observations correctly predicted, and the total number of positive observations predicted. *Recall* is the ratio of predicted positive observations to all observations in the true class. The *F1 score* is an effective metric for evaluating segmentation, allowing us to interpret the balance between precision and recall of the overlapping pixels between the ground truth and the result of the method.

3. Results and discussion

In this study, two different segmentation methods, fuzzy logic based and CNN based active contour method, which are applied for the first time for tooth segmentation, are introduced and compared with existing methods in the literature. The experimental studies were conducted using the MATLAB programming language. The computational experiments were performed on a computer equipped with an i5 2.5 GHz processor, an Intel (R) HD Graphics 3000 2GB GPU card, and 4GB RAM.

3.1. Edge detection with fuzzy logic

The results obtained after applying the 16 fuzzy rules to X-ray 1 and X-ray 2 images are depicted in Figure 10. As detailed in Table 3, the performance of the coefficients utilized for determining the threshold value in edge detection varies due to the structural disparities of the jaw. The careful selection of the most appropriate coefficients for the active contour method significantly impacts the effectiveness of edge detection.

F1 score is known as a metric used to evaluate the performance of a classification or segmentation algorithm (Alfonso-Francia et al., 2022). The F1 score parameter was used as the primary metric for comparing the performance of coefficients, taking into account the density of the black areas and providing an indication of the accuracy of the white pixels. Among the parameters with the same F1 score value (1.151), the *k* and *l* parameters with the highest Recall value (0.242) were chosen.
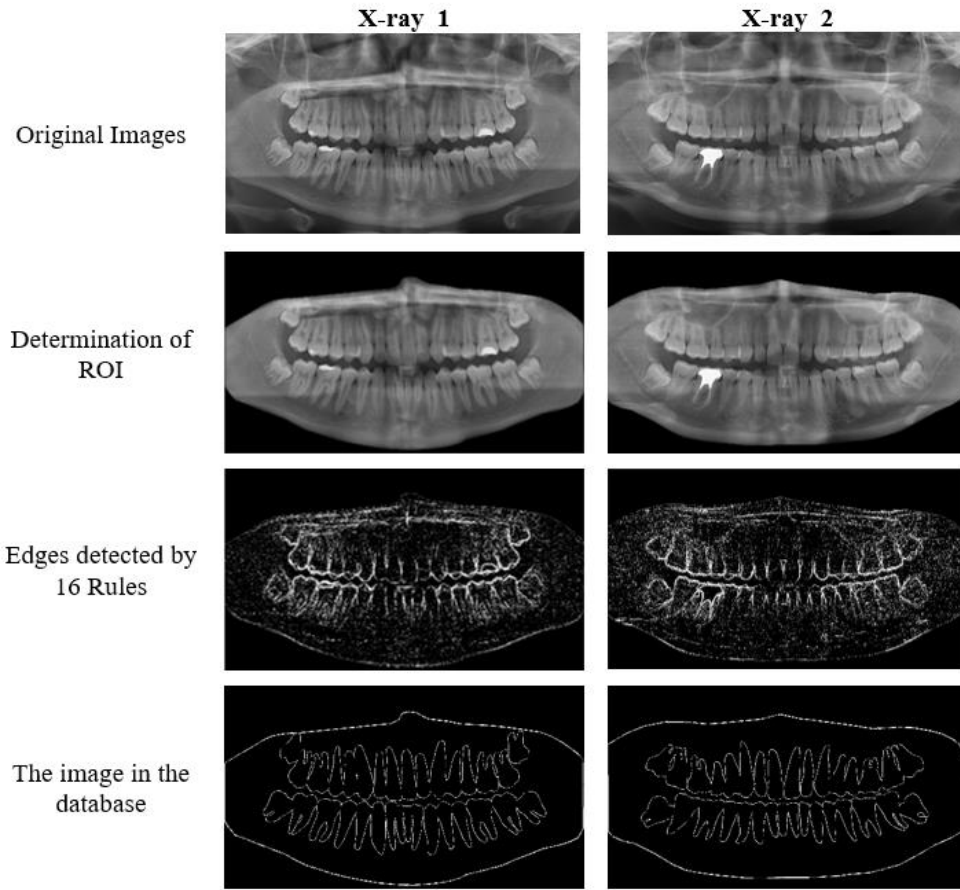
Figure 10. Results After 16 Fuzzy Rules on X-ray 1 & 2 and Database Comparison

The proposed fuzzy logic edge detection method is compared to three methods: Sobel, Prewitt, and Canny. Sobel and Prewitt methods rely on approximating the gradient magnitudes within images. The Sobel method concentrates on gradients around each pixel, determining the final gradient by computing gradients in both the *x* and *y* directions (Das, 2016).

Table 3. Performance evaluation according to change of coefficients

| Image	k	l	Accuracy	Specificity	Precision	Recall	F1 score
X-ray 1	0.5	0.5	0.967	0.998	0.121	0.009	0.017
	0.6	0.4	0.938	0.963	0.133	0.177	0.151
	0.7	0.3	0.927	0.950	0.119	0.208	0.151
	0.8	0.2	0.915	0.937	0.110	0.242	**0.151**
	0.9	0.1	0.894	0.913	0.099	0.296	0.149
	1	0	0.882	0.900	0.094	0.319	0.145
	0.5	0	0.780	0.791	0.065	0.449	0.113
	0.6	0	0.814	0.827	0.071	0.412	0.122
	0.7	0	0.848	0.863	0.081	0.373	0.133
	0.8	0	0.882	0.900	0.094	0.319	0.145
X-ray 2	0.5	0.5	0.969	0.999	0.081	0.003	0.006
	0.6	0.4	0.969	0.999	0.084	0.005	0.009
	0.7	0.3	0.968	0.998	0.086	0.008	0.014
	0.8	0.2	0.948	0.972	0.148	0.161	0.154
	0.9	0.1	0.939	0.962	0.132	0.189	**0.156**
	1	0	0.928	0.950	0.119	0.221	0.154
	0.5	0	0.830	0.844	0.069	0.379	0.117
	0.6	0	0.871	0.888	0.083	0.330	0.133
	0.7	0	0.903	0.922	0.099	0.282	0.148
	0.8	0	0.928	0.950	0.119	0.221	0.154

Similarly, the Prewitt operator detects horizontal and vertical edges in images. In contrast to the Sobel, this operator does not emphasize pixels closer to the mask's center. By thresholding the gradient magnitude, they also generate a binary image of edge detections. On the other hand, the Canny method calculates the gradient of the input image using the derivative of the Gaussian filter. It identifies edges based on gradient maxima and utilizes two thresholds to distinguish strong and weak edges. Weak edges are considered in the output only if they are connected to strong edges. Experimental results, as presented in Table 4, demonstrate the superiority of the proposed method over existing ones.

Table 4. Comparison of methods

Image		Accuracy	Specificity	Precision	Recall	F1 score
	Sobel	0.964	0.993	0.229	0.057	0.092
	Canny	0.897	0.921	0.056	0.146	0.081
	Prewitt	0.964	0.993	0.231	0.058	0.092
	Proposed	0.915	0.936	0.110	0.241	**0.151**
	Sobel	0.967	0.995	0.274	0.059	0.097
	Canny	0.919	0.943	0.070	0.139	0.093
	Prewitt	0.967	0.995	0.274	0.059	0.097
	Proposed	0.938	0.961	0.132	0.189	**0.156**

3.2. Segmentation with CNN

Figure 11 shows the block diagram of the CNN method for segmentation of the tooth region. After determining the ROI region from the image, the mask image to be used in the active contour method is obtained with the proposed CNN architecture. Using the ROI image and the mask image, which is the CNN output, the segmented image, which is the active contour output, is obtained.
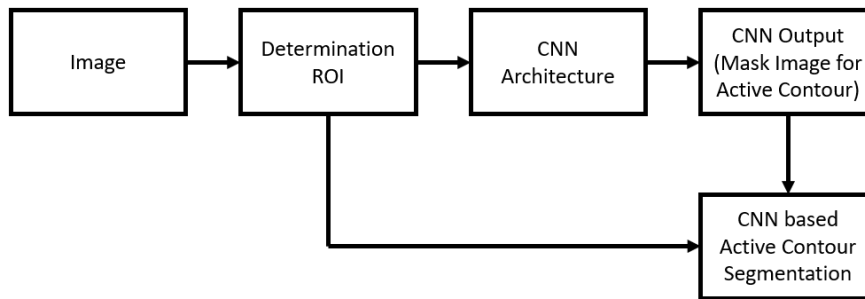
Figure 11. Block diagram of segmentation with CNN active contour method

In CNN, 70% of the dataset is devoted to training, while 30% is devoted to testing (Hakim et al., 2022). This model uses 2000 as the training step (epoch), 32 as the batch size, and 0.0001 as the learning coefficient (learning rate). Figure 12 shows some of the images tested as a result of the convolutional neural network.
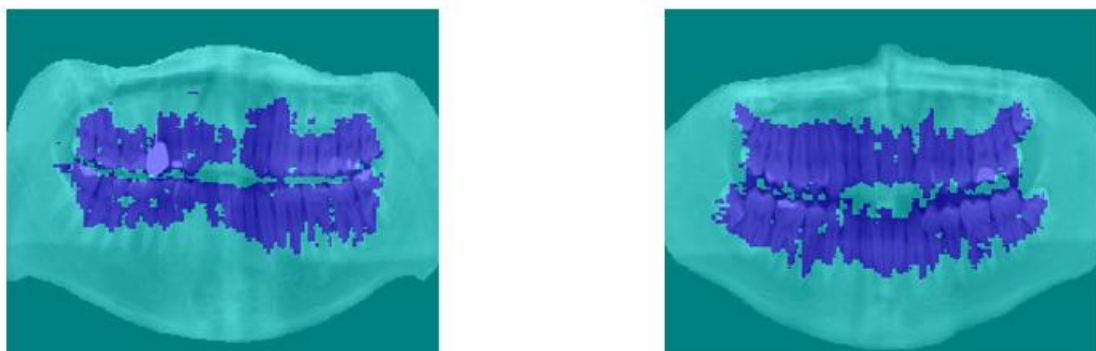
Figure 12. Output of CNN for X-ray 1 and X-ray 2

Convolutional neural network testing was conducted on a dataset consisting of 220 images. Performance evaluation results for each tested image are summarized in Table 5, presenting the average values derived from the comprehensive analysis.

Table 5. Performance evaluations of tested images

Method	Accuracy	Specificity	Precision	Recall	F1 score
CNN	0.9695±0.03	0.9852±0.02	0.1460±0.09	0.1322±0.08	0.1349±0.09

3.3 Image segmentation with fuzzy active contour model and CNN active contour model

When using the active contour method, it is usually necessary to use a mask image. This mask image, combined with the initial contour and an energy function, helps accurately find the boundaries of the object. So, in active contouring, picking and creating the right mask image are crucial steps. A well-designed mask image is important for getting precise and effective segmentation results. In this study, mask images are generated using both Convolutional Neural Network (CNN) and Fuzzy rules. Subsequently, these generated mask images are employed in the segmentation process through the active contour method. The obtained output result shown in Figure 13.
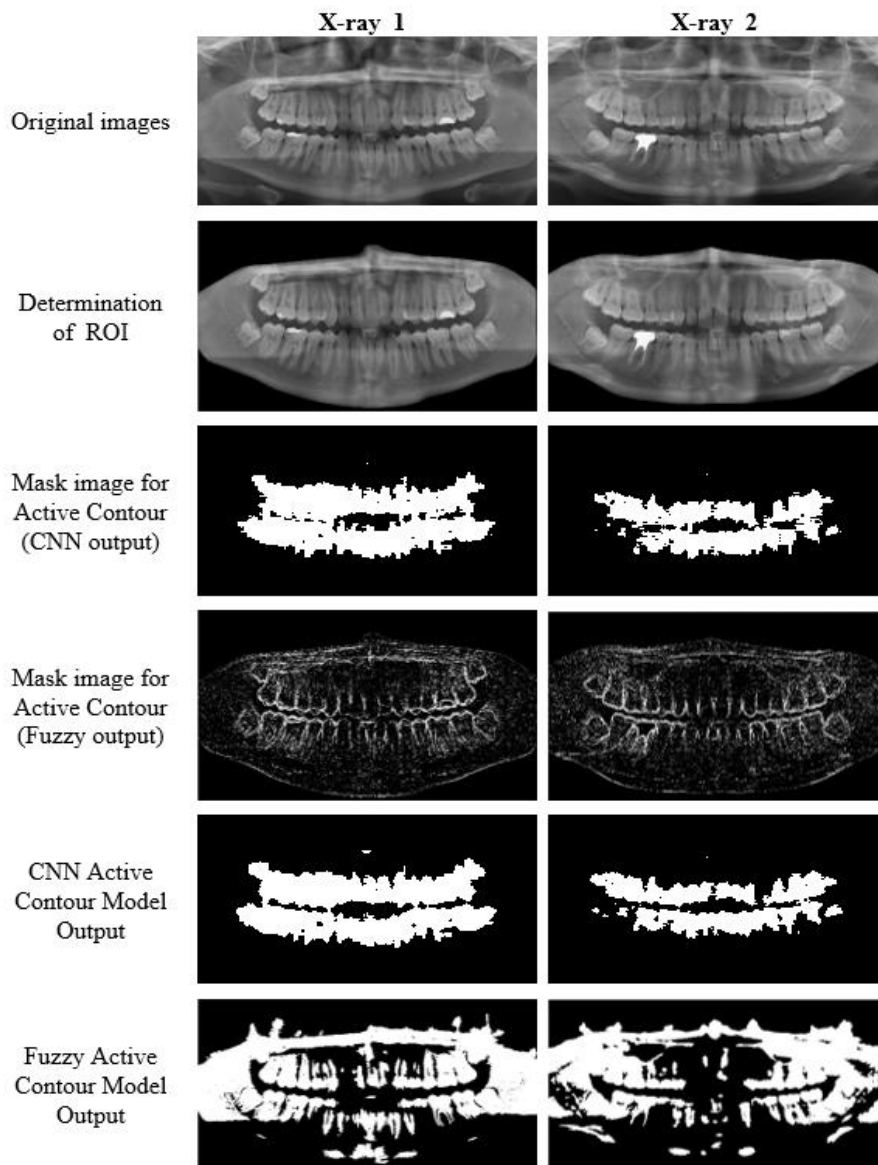
Figure 13. Image Segmentation with Fuzzy Active Contour Model and CNN Active Contour Model

Table 6 shows the performance values obtained by comparing the retrieved images with the reference images in the dataset. According to the Table 6, the CNN-Based Active Contour method emerges as the most precise. This conclusion is supported by the superior image accuracy achieved with this method. Furthermore, the CNN-Based Active Contour method demonstrates the highest level of specificity. The comparison images indicate that the method accurately identifies the black pixels. Analyzing the results for precision, recall, and F1 score, it becomes evident that segmentation using the Fuzzy-Based Active Contour stands out as the most effective approach. This success underscores the method's proficiency in identifying the white pixels, specifically the tooth region of the image.

Table 6. Performance evaluation

Method	Accuracy	Specificity	Precision	Recall	F1 score
Fuzzy based active Contour	0.7198	0.8731	**0.6246**	**0.4169**	**0.5000**
CNN based active Contour	**0.9706**	**0.9872**	0.1135	0.0870	0.0944

3.4 Discussion

The segmentation of the tooth region from dental X-ray images holds significant importance in various dental applications, as well as in bone age estimation and forensic dentistry (Bologna et al., 2023). In this study, a combination of fuzzy logic and a CNN-based active contour method is used to automatically segment the tooth region. Similar studies with the same objective can be found in the literature.

Kumar et al. (2019) conducted tooth region segmentation using a new semi-supervised model employing the Fuzzy C-Means algorithm. They emphasized that the proposed method improved performance by 3%-30% compared to traditional methods. Datta et al. (2023) reported achieving 93.2% accuracy in automatically segmenting tooth regions from dental X-ray images using Fuzzy C-Means. Silva et al. (2018) utilized the Mask RCNN method for segmentation and achieved an accuracy of 0.9208, specificity of 0.9612, precision of 0.8373, sensitivity of 0.7619, and F1 score of 0.7944, consistent with their findings. The FCN method applied by Koch et al. (2019) yielded an accuracy of 0.9521, specificity of 0.9614, precision of 0.9331, sensitivity of 0.9437, and F1 score of 0.9363. Zhao et al. (2020) obtained an accuracy of 0.9694, specificity of 0.9781, precision of 0.9497, sensitivity of 0.9377, and F1 score of 0.9272 using the CNN architecture named TSASNet. Lee et al. (2020) reported a sensitivity of 0.893, precision of 0.858, and F1 score of 0.875 with R-CNN, while Da Silva Rocha et al. (2022) achieved an accuracy of 0.9659, precision of 0.9301, sensitivity of 0.9270, and F1 score of 0.9287 with the DoubleU-NET method.

The Fuzzy-Based Active Contour method demonstrates moderate accuracy (0.7198), acceptable specificity (0.8731), and precision (0.6246), showing robust performance despite some areas for improvement. The CNN-Based Active Contour method stands out with very high accuracy (0.9706) and specificity (0.9872). These developed methods are generally competitive with existing approaches, and integrating the strengths of these methods in future studies could lead to more balanced and high-performance segmentation methods.

4. Conclusion

In this study, tooth segmentation from radiographs was conducted using two distinct methods: fuzzy rule-based edge detection followed by the active contour method, and a CNN-based active contour method. Both approaches demonstrated notable efficacy in segmenting tooth regions, albeit with different strengths. The fuzzy rule-based edge detection, coupled with the active contour method, accurately identified segmented tooth regions by utilizing edge pixels as a mask. The method achieved a precision value of 0.6246, a recall value of 0.4169, and an F1 score of 0.50. This approach effectively captured the tooth edges, contributing to precise segmentation. On the other hand, the CNN-based active contour method excelled in overall pixel accuracy and the detection of non-tooth pixels, achieving an accuracy value of 0.9706 and a specificity value of 0.9872. The deep learning capabilities of the CNN allowed for detailed and accurate segmentation, highlighting its potential for high-performance applications. Given the primary objective of providing insights for dentists regarding tooth roots, fractures, and wear patterns, neither method can be conclusively favored over the other. Each method presents unique advantages that can be leveraged for different aspects of dental analysis. The potential for enhanced performance exists if these methods are used in conjunction or as part of a comprehensive approach. Overall, this study demonstrates that both fuzzy rule-based and CNN-based active contour methods

are effective tools for tooth segmentation in radiographs. Future work could explore the integration of these methods to maximize their strengths, offering a more robust solution for dental imaging analysis.

Author contribution

SK: supervision, article administration, and resources. FD and FÖ; methodology and writing-original draft preparation. FD and FÖ; writing, reviewing, and editing.

Declaration of ethical code

The authors of this article declare that the materials and methods used in this study do not require ethical committee approval and/or legal-specific permission.

Conflicts of interest

The authors declare that there is no conflict of interest

References

Adejoh, T., Ewuzie, O. C., Ogbonna, J. K., Nwefuru, S. O., & Onuegbu, N. C. (2016). A derived exposure chart for computed radiography in a negroid population. *Health*, *8*(10), 953-958. https://doi.org/10.4236/health.2016.810098

Alfonso-Francia, G., Pedraza-Ortega, J.C., Badillo-Fernández, M., Toledano-Ayala, M., Aceves-Fernandez, M.A., Rodriguez-Resendiz, J., Ko, S.-B., & Tovar-Arriaga, S. (2022). Performance Evaluation of Different Object Detection Models for the Segmentation of Optical Cups and Discs. Diagnostics, 12, 3031. https://doi.org/10.3390/diagnostics12123031

Bologna M., Michaela, C., Maurizio, C., Deborah, F.., Sergio, P.., Marco, A. (2023). Teeth Segmentation in Panoramic Dental X-ray Using Mask Regional Convolutional Neural Network. Applied Sciences, 13(13):7947-7947. doi: 10.3390/app13137947

Bozkurt, M. H., & Karagol, S. (2020). Jaw and Teeth Segmentation on the Panoramic X-Ray Images for Dental Human Identification. *Journal of digital imaging*, *33*(6), 1410–1427. https://doi.org/10.1007/s10278-020-00380-8

Bruellmann, D., Sander, S., & Schmidtmann, I. (2016). The design of an fast Fourier filter for enhancing diagnostically relevant structures - endodontic files. *Computers in Biology and Medicine*, *72*, 212–217. https://doi.org/10.1016/j.compbiomed.2016.03.019

Cheng, C., Chen, Y. & Jiang, X. (2000). Thresholding using two-dimensional histogram and fuzzy entropy principle. *IEEE Transactions on Image P*rocessing, *9*(4), 732-735, https://doi.org/10.1109/83.841949

Cheng, H-D., & Xu, H. (2002). A novel fuzzy logic approach to mammogram contrast enhancement. *Information Sciences*, *148*(1-4), 167-184. https://doi.org/10.1016/S0020-0255(02)00293-1

Celeghin, A., Borriero, A., Orsenigo, D., Diano, M., Méndez Guerrero, C. A., Perotti, A., ... & Tamietto, M. (2023). Convolutional neural networks for vision neuroscience: Significance, developments, and outstanding issues. Frontiers in Computational Neuroscience, 17, 1153572. https://doi.org/10.3389/fncom.2023.1153572

Da Silva Rocha, É., & Endo, P. T. (2022). A comparative study of deep learning models for dental segmentation in panoramic radiograph. Applied Sciences, 12(6), 3103. https://doi.org/10.3390/app12063103

Das, S. (2016). Comparison of Various Edge Detection Technique. *International Journal of Signal Processing, Image Processing and Pattern Recognition*, *9*(2), 143-158. https://dx.doi.org/10.14257/ijsip.2016.2.13

Datta, S., Chaki, N., Modak B. (2023). A novel technique for dental radiographic image segmentation based on neutrosophic logic. Decision Analytics Journal, 7, 100223. https://doi.org/10.1016/j.dajour.2023.100223

Dhanachandra, N. & Chanu, Y. J. (2020). An image segmentation approach based on fuzzy c-means and dynamic particle swarm optimization algorithm. *Multimedia Tools and Applications*, *79*, 18839-18858, https://doi.org/10.1007/s11042-020-08699-8

Gómez, D., Montero, J., & Yanez, J. (2006). A coloring fuzzy graph approach for image classification. *Information Sciences*, *176*(24), 3645-3657, https://doi.org/10.1016/j.ins.2006.01.006

Hakim, W. L., Rezaie, F., Nur, A. S., Panahi, M., Khosravi, K., Lee, C. W., & Lee, S. (2022). Convolutional neural network (CNN) with metaheuristic optimization algorithms for landslide susceptibility mapping in Icheon, South Korea. Journal of environmental management, 305, 114367. https://doi.org/10.1016/j.jenvman.2021.114367

Hashemi, S. E., Jouybari, F. G., & Keshteli, M. H. (2023). A fuzzy C-means algorithm for optimizing data clustering. *Expert Systems With Applications*, *227*, 1-14. https://doi.org/10.1016/j.eswa.2023.120377

Hoang, H. H., & Tran, B. L. (2021). Accurate instance-based segmentation for boundary detection in robot grasping application. *Applied Sciences*, *11*(9), 1-15. https://doi.org/10.3390/app11094248

Hu, L., Cheng, H-D., & Zhang, M. (2007). A high performance edge detector based on fuzzy inference rules. *Information sciences*. *177*(21), 4768-4784, https://doi.org/10.1016/j.ins.2007.04.001

Jain, K. R., & Chauhan, N. C. (2019). *Dental Image Analysis for Disease Diagnosis* (1st ed., pp. 59-83). Springer Cham. https://doi.org/10.1007/978-3-030-14136-3

Kaseva, T., Omidali, B., Hippeläinen, E., Mäkelä, T., Wilppu, U., Sofiev, A., Merivaara, A., Yliperttula, M., Savolainen, S., & Salli, E. (2022). Marker-controlled watershed with deep edge emphasis and optimized H-minima transform for automatic segmentation of densely cultivated 3D cell nuclei. *BMC Bioinformatics*, *23*(1), 289. https://doi.org/10.1186/s12859-022-04827-3

Kass, M., Witkin, A., & Terzopoulos, D. (1988). Snakes: Active Contour Models. *International Journal of Computer Vision*, *1*(4), 321-331. https://doi.org/10.1007/BF00133570

Khalid, N. (2022). Review on region-based segmentation using watershed and region growing techniques and their applications in different fields. *Journal La Multiapp*, *3*(5), 241-249. https://doi.org/10.37899/journallamultiapp.v3i5.714

Koch, T. L., Perslev, M., Igel, C. & Brandt, S. S. (2019). Accurate Segmentation of Dental Panoramic Radiographs with U-NETS. 2019 IEEE 16th International Symposium on Biomedical Imaging (ISBI 2019), Venice, Italy, pp. 15-19, doi: 10.1109/ISBI.2019.8759563.

Kumar, A., Bhadauria, H.S. & Singh, A. (2020). Semi-supervised OTSU based hyperbolic tangent Gaussian kernel fuzzy C-mean clustering for dental radiographs segmentation. Multimed Tools Appl 79, 2745–2768. https://doi.org/10.1007/s11042-019-08268-8

Kumar, A., Bhadauria, H. S., & Singh, A. (2021). Descriptive analysis of dental X-ray images using various practical methods: A review. *PeerJ. Computer science*, *7*, e620. https://doi.org/10.7717/peerj-cs.620

Lee, J. H., Han, S. S., Kim, Y. H., Lee, C., & Kim, I. (2020). Application of a fully deep convolutional neural network to the automation of tooth segmentation on panoramic radiographs. Oral surgery, oral medicine, oral pathology and oral radiology, 129(6), 635-642. https://doi.org/10.1016/j.oooo.2019.11.007

Li, C., Kao, C. Y., Gore, J. C., & Ding, Z. (2008). Minimization of region-scalable fitting energy for image segmentation. *IEEE transactions on image processing: a publication of the IEEE Signal Processing Society*, *17*(10), 1940–1949. https://doi.org/10.1109/TIP.2008.2002304

Long, J., Shelhamer, E., & Darrell, T. (2015). Fully convolutional networks for semantic segmentation. *2015 IEEE Conference on Computer Vision and Pattern Recognition (CVPR),* (pp. 3431-3440), Boston, MA, USA. https://doi.org/10.1109/CVPR.2015.7298965

Milletari, F., Navab, N. & Ahmadi, S-A. (2016). V-net: Fully convolutional neural networks for volumetric medical image segmentation. *In: 2016 fourth international conference on 3D vision (3DV)*, (pp. 565-571), Stanford, CA, USA, https://doi.org/10.1109/3DV.2016.79

Minnema, J., van Eijnatten, M., Hendriksen, A. A., Liberton, N., Pelt, D. M., Batenburg, K. J., Forouzanfar, T., & Wolff, J. (2019). Segmentation of dental cone-beam CT scans affected by metal artifacts using a mixed-scale dense convolutional neural network. *Medical physics*, *46*(11), 5027–5035. https://doi.org/10.1002/mp.13793

Mitra, S. (2021). A scanner smartly. *Significance*, *18*(3), 12–17, https://doi.org/10.1111/1740-9713.01526

Polizzi, A., Quinzi, V., Ronsivalle, V., Venezia, P., Santonocito, S., Lo Giudice, A., Leonardi, R., & Isola, G. (2023). Tooth automatic segmentation from CBCT images: a systematic review. *Clinical oral investigations, 27*(7), 3363–3378. https://doi.org/10.1007/s00784-023-05048-5

Ramachandran, R., Gobalakrishnan, N. & Chokkalingam, A. (2022). A Survey on Various Medical Image Classification and Feature Recognition Techniques. *2022 6th International Conference on Trends in Electronics and Informatics (ICOEI)*, (pp. 1518-1526), Tirunelveli, India, https://doi.org/10.1109/ICOEI53556.2022.9777207

Sezgin, M., & Sankur, B. (2004). Survey over image thresholding techniques and quantitative performance evaluation. *Journal of Electronic Imaging*, *13*(1), 146-166. https://doi.org/10.1117/1.1631315

Silva, S., Oliveira, L., & Pithon, M. (2018). Automatic segmenting teeth in X-ray images: Trends, a novel data set, benchmarking and future perspectives. *Expert Systems With Applications*, *107*, 15-31. https://doi.org/10.1016/j.eswa.2018.04.001

Thakkar, P., Patel, D., Hirpara, I., Jagani, J., Patel, S., Shah, M., & Kshirsagar, A. (2023). A Comprehensive Review on Computer Vision and Fuzzy Logic in Forensic Science Application. *Annals of Data Science*, *10*, 761-785. https://doi.org/10.1007/s40745-022-00408-6

Thias, A.H., Al Mubarok, A.F., Handayani, A., Danudirdjo, D. & Rajab, T.E. (2019). Brain tumor semi-automatic segmentation on mri t1-weighted images using active contour models. *In: 2019 International Conference on Mechatronics, Robotics and Systems Engin*eering (MoRSE). (pp. 217-221), Bali, Indonesia, https://doi.org/10.1109/MoRSE48060.2019.8998651

Zhang, Y., Zhang, J., & Zhou, W. (2022). Research on Image Classification Improvement Based on Convolutional Neural Networks with Mixed Training. *2022 IEEE 4th International Conference on Civil Aviation Safety and Information Technology (ICCASIT)*, (pp. 7-10), Dali, China. https://doi.org/10.1109/ICCASIT55263.2022.9986643

Zhao, Y., Li, P., Gao, C., Liu, Y., Chen, Q., Yang, F., & Meng, D. (2020). TSASNet: Tooth segmentation on dental panoramic X-ray images by Two-Stage Attention Segmentation Network. Knowledge-Based Systems, 206, 106338.